

Article

Quantifying the Spatio-Temporal Pattern Differences in Climate Change before and after the Turning Year in Southwest China over the Past 120 Years

Meng Wang ^{1,*} , Shouyan Wang ² and Zhengfeng An ³ ¹ Chaozhou Environmental Information Center, Chaozhou 521011, China² School of Life Science and Engineering, Handan University, Handan 056005, China³ Department of Renewable Resources, University of Alberta, Edmonton, AB T6G 2E3, Canada

* Correspondence: wangmengzhisha@126.com

Abstract: In conjunction with Earth's ongoing global warming, the Southwest China (SWC) region has become a fascinating case study on the control of local climate change. Moreover, an entire period of climate change may partially mask the patterns in some stages. Therefore, in this research, we investigated the spatial patterns of the significant turning years of climatic factor change, and determined the heterogeneity of the spatial patterns of climate change before and after the significant turning years. We used the long time-series of the CRU datasets (CRU_TS4.02) from 1901 to 2017 with a piecewise linear regression model to explore the significant turning-year distribution characteristics of inter-annual and inter-seasonal climate factor changes, and further describe and quantize the differences in the spatio-temporal patterns of climate factors before and after the significant turning years on the grid scale in SWC. Overall, the trends in temperature and precipitation factors in SWC were segmented over the last 120 years, with significant turning years with different regional and stepwise characteristics. In terms of timing, temperature and precipitation factors changed significantly in 1954 and 1928, respectively, and overall temporal variability ($0.04\text{ }^{\circ}\text{C}/(10\text{ a})$ ($p < 0.05$), $-0.48\text{ mm}/(10\text{ a})$) masked the magnitude or direction of variability ($0.13\text{ }^{\circ}\text{C}/(10\text{ a})$ and $0.16\text{ }^{\circ}\text{C}/(10\text{ a})$ both at the level of $p < 0.05$ before the turning year, $19.56\text{ mm}/(10\text{ a})$ ($p < 0.05$) and $1.19\text{ mm}/(10\text{ a})$ after the turning year) around the watershed years. Spatially, the significant turning years were concentrated in the periods 1940–1993 (temperature) and 1910–2008 (precipitation), and the distribution pattern of the turning years was patchy and concentrated. The turning years of temperature factors were gradually delayed from east to west, and the variability of climate factors before and after the turning years exhibited significant shifts in location (e.g., temperature decreased from southeast to northwest before the turning year and increased after the turning year). After the turning year, the warming variability of the temperature factor increased, while the increasing variability of the precipitation factor decreased. Further integrated analysis revealed that the increase in variability of the climate factor after the turning year was mainly due to the increase in winter and autumn variability ($0.05\text{ }^{\circ}\text{C}/(10\text{ a})$, $7.30\text{ mm}/(10\text{ a})$ in autumn; and $0.12\text{ }^{\circ}\text{C}/(10\text{ a})$, $1.97\text{ mm}/(10\text{ a})$ in winter). To the extent that this study provides a necessary academic foundation for efficiently unveiling the spatio-temporal variability properties of climate factors against the background of modern global climate change, more attention should be paid to the location and phase of the study.

Keywords: southwestern China; turning year; piecewise linear regression; spatio-temporal pattern

Citation: Wang, M.; Wang, S.; An, Z. Quantifying the Spatio-Temporal Pattern Differences in Climate Change before and after the Turning Year in Southwest China over the Past 120 Years. *Atmosphere* **2023**, *14*, 940. <https://doi.org/10.3390/atmos14060940>

Academic Editor: Agnieszka Krzyżewska

Received: 11 April 2023

Revised: 21 May 2023

Accepted: 25 May 2023

Published: 27 May 2023



Copyright: © 2023 by the authors. Licensee MDPI, Basel, Switzerland. This article is an open access article distributed under the terms and conditions of the Creative Commons Attribution (CC BY) license (<https://creativecommons.org/licenses/by/4.0/>).

1. Introduction

Nearly all areas of Earth's land surface have experienced unprecedented warming processes over the past century [1–11], and warming has continued to accelerate, particularly over the last 50 years [1,8,11–13]. In the last 30 years, the warming of Earth's surface has been the highest since 1850, and global land warming is predicted to rise by $1.5\text{ }^{\circ}\text{C}$ and $3\text{--}12\text{ }^{\circ}\text{C}$ by the mid- and late-21st century, respectively [2,3,9,13–18]. However, there

is remarkable inhomogeneity in time and space and considerable heterogeneity in the temperature variability between different global latitudes [4]. Warming trends are stronger in the mid- and high-latitude areas of the Northern Hemisphere and weaker in the Southern Hemisphere and tropics. The North Asian region from Siberia to Mongolia has shown the most drastic warming over the last hundred years, with the warming rate exceeding $2\text{ }^{\circ}\text{C}/(100\text{ a})$ [12,15–17,19,20], and the global annual mean land surface temperature showing a more significant warming trend in the first 20 years of the new century; however, spatial differences have been more significant [21–23]. The situation described above has led to a further increase in the intensity and number of extreme weather events worldwide, resulting in accelerated glacial melting, significant cryospheric retreat, significant reductions in the quantity and acreage of snowpack, and rapid sea-level rise, altering the quantity and quality of rivers, lakes, and wetlands [6,8–11,14,24] and ultimately affecting the distribution pattern of global precipitation [16,25–27]. For example, mid- and high-latitude regions in the Northern Hemisphere, tropical regions, and subtropical regions in the Southern Hemisphere have shown a significantly increasing precipitation trend [25,26]. There has been a decreasing precipitation trend in the warm temperate climate regions and an increasing trend in the arid and polar climate regions [28]. Precipitation has increased since 1950 over the mid-latitude and northern regions of Eurasia, southeastern South America, the central United States, and northwestern Australia [27,29], while it has decreased [27,29,30] in much of Africa, southern Europe, East Asia, South Asia, the Mediterranean, and the high latitudes. Studies of climate change patterns in China, a region sensitive to global climate change, also indicate a significant upward trend in overall temperatures, with the country warming faster than the global mean value over the corresponding period [10,31]. In addition, research on the pattern of climatic variation in China has shown that the areas with significant warming are mainly concentrated in mid- and high-latitude regions [32], and the recorded warming rate has been as high as $0.27\text{ }^{\circ}\text{C}/(10\text{ a})$ [33]. Although there have been no discernible trends in inter-annual precipitation in China, there have been pronounced regional differences in precipitation changes, and most of the western regions, especially the northwestern region, have experienced an increase in precipitation, while the eastern area of the northwest, most of Northern China, parts of the southwest, and the southern area of the northeastern region have decreased [34–36]. The warming rate of the average annual temperature of the Qinghai–Xizang Plateau increased significantly from 1970 to 2015 by $0.044\text{ }^{\circ}\text{C}/\text{a}$ ($p < 0.05$), and the overall precipitation increased weakly and significantly at a rate of $0.50\text{ mm}/\text{a}$ ($p < 0.1$), showing a significant increasing trend in the central and northeastern regions, while showing a significant decreasing trend in the eastern and southeastern regions. Moreover, the number and intensity of extreme weather events have also increased. For example, dry days and heavy rainfall increased by $3.78\%/ (10\text{ a})$ and $1.51\%/ (10\text{ a})$, respectively, from 1960 to 2013 [37].

In general, strong correspondence between the climate and biomes has been demonstrated, and climate zones can generally be considered proxies for vegetation distribution [38–41]. When climatic zones increase/decrease rapidly, they alter the distribution range of suitable vegetation and the seasonal activity required to maintain its ecological niche [39,40,42]. Similar studies have shown that temperature increases have led to changes in the distribution of some vulnerable climate scenarios. In particular, a dramatic expansion of the temperate climate class in the temperate zone has been reported since 1950, with the most significant climate change occurring from continental to temperate among all climate scenarios [39,40,43]. Other studies have verified that the heterogeneity of vegetation spatial patterns could alleviate regional and even global climate change by adjusting the biogeochemical properties of the surface energy balance and carbon cycle [44–48]. Over the last three decades, biophysical feedback associated with global greening has slowed global surface warming by about 12% [45], and the average terrestrial biophysical warming caused by forest loss has reached 18% of the global biogeochemical signal caused by CO_2 [46]. Increases in vegetation cover in central and western Europe have also led to a $0.12 \pm 0.20\text{ }^{\circ}\text{C}$ decrease in mean summer and autumn temperatures [47]. The fifth IPCC

report [1] showed that increasing vegetation cover would reduce surface radiative forcing by $0.15 \pm 0.10 \text{ Wm}^{-2}$. In-depth research has shown that most scientists in recent decades have gradually come to view regions at higher elevations as “early warning systems” and amplifiers of global climate change [49–55], especially exploring the relationship between warming and wetting rates and altitude, i.e., the problem of elevation-dependent warming and elevation-dependent wetting. In addition, studies on the Qinghai–Xizang Plateau [55], the Andes [51], the Colorado Rockies [53], and the Yunnan Plateau [52] have found that the warming rate is significantly greater at higher elevations than at lower elevations. Southwest China (SWC) has elevation differences of thousands of orders of magnitude and is simultaneously influenced by both monsoon and westerly winds, leading to the heterogeneity of the distribution pattern of climate conditions being more colorful, overlapping the different types of vegetation and vegetation cover (Figure 1b), and making SWC a typical case for controlling local climate change. Moreover, the results of analyzing trends in one period are not transferable to another. Observations over an entire period may obscure some detailed patterns of climate change that vary over time. Most previous studies have focused on trends in climate change over an entire period or looked at changes in climate over a given period of the last 50 years [1,8,11–13], 30 years [2,3,13–17], 20 years [21–23], 10 years [18], or 5 years [9] compared to trends over an entire period, especially since 1850 or 1850–1900 [2,3,13–17]. Nevertheless, there are often distinct phases of climatic factor change—that is, there are different trends in climatic factor change over different periods. Therefore, in order to more accurately describe the spatio-temporal dynamic characteristics of climate change in SWC over the past 120 years, and reveal the distribution characteristics and differences in climatic factors before and after the turning year at the grid level, we put forward the following scientific problems: (1) How can we reveal the significant turning year and its climatic factor distribution characteristics? (2) How can we describe and quantify differences in the spatial patterns of climate change before and after the significant turning year of climate factors?

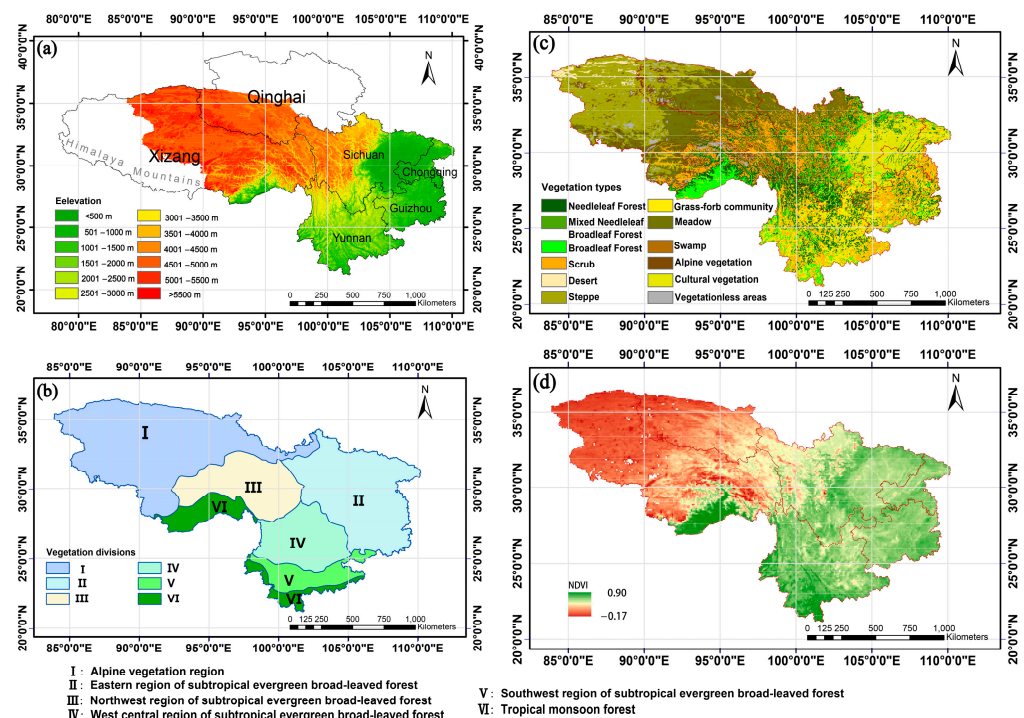


Figure 1. Overview of (a) geography, (b) vegetation divisions, (c) vegetation types, and (d) NDVI in the SWC area. The net space in panel (a) refers to regions within the provinces that were not included in the scope of this study.

Therefore, we referred to the practice of Wang [56] and introduced the “turning year” to solve the related problems. Specifically, piecewise linear regression was chosen to find a breakpoint, and linear fitting was performed before and after each breakpoint. The breakpoints and slopes with the smallest sum of squares of the fitted residuals were selected as the optimal solution of the piecewise fits. The significance of the turning year of the climate factor was then tested by constructing the classical *F*-test theory. Further quantitative analysis revealed significant turning years, and we undertook an in-depth exploration of related phenomena and causes. Therefore, in order to comprehensively understand the spatial-temporal changes in climatic factors in SWC over the past 120 years, we used long time-series CRU data from 1901 to 2017 and explored the significant turning years and their distribution characteristics in respect of the inter-annual and inter-seasonal climate change. We further described and quantified the differences in spatial patterns before and after the significant turning years. To some extent, it is necessary to pay more attention to clarifying the period and the distribution location of the study to effectively reveal the spatial-temporal variations in long-term climatic factor data series.

2. Materials and Methods

2.1. Overview of the Research Area

With reference to the commonly used concept of natural regeneration [57,58], the region of SWC covered by this study has a broader geographical meaning that attaches importance to vegetation and landscape features, and the geographical coordinates range from 21.14 to 36.48° N and 83.87 to 110.19° E. Geomorphologically, SWC is dominated by the Himalayas, the Qinghai–Xizang Plateau (QX–P), the Hengduan Mountains (HD–M), the Yunnan–Guizhou Plateau (YG–P), and the Sichuan Basin (SC–B). The terrain has a pattern of decreasing elevation from the west and northwest to the east and southeast [44,59,60], with elevation differences of thousands of orders of magnitude, encompassing the three primary levels of Chinese topography (Figure 1a). In addition, the uplift of the Himalayas, which blocks the warm and humid monsoon from the Indian Ocean monsoon, creates the unique climate of the QX–P. The QX–P is under the influence of the South Asian monsoon, East Asian monsoon, and westerly winds, which have an essential impact on the regional and global climate of East Asia, making the QX–P a key research area [11,44,58–60] and a fascinating case study for local climate change control [1,24,53,58]. The annual mean temperature gradually increases from the northwest (less than 0 °C) to the southeast (more than 24 °C) and is constrained by topographic and climatic factors. The spatio-temporal distribution of precipitation resources is highly inhomogeneous, decreasing from southeast to northwest, with minimum and maximum values differing by thousands of millimeters [61], and precipitation is mainly concentrated in the period April to September, with distinct dry and wet seasons.

2.2. Obtaining and Analyzing the Research Data

2.2.1. Data Sources and Processing

- (1) The high-resolution gridded dataset (CRU_TS4. 02) of climate variables used in this study was downloaded from the Institute of Climate Research, University of East Anglia (see Table 1), and its time range covers the period 1901 to 2017 (117 years \times 12 months = 1404 months in total) with a resolution of 0.5° \times 0.5°. The dataset has been integrated with several well-known databases to re-construct a complete, high-resolution, uninterrupted dataset of surface climate elements [62], and it is often used as a reliable source of climate information when considering the global or regional shaping of climate change and associated environmental impacts [44,59,63]. Moreover, this dataset is consistent with the interannual variability sequence of China’s mean annual temperature and annual precipitation, which can be used to analyze China’s century-long climate change [64]. As SWC spans three terrain zones from west to east, the transition between adjacent zones is scattered (Figure 1a), and the different elevations have significant climatic features (such as

elevation-dependent warming [49] and elevation-dependent wetting [50]); meteorological data with a spatial resolution of $0.5^\circ \times 0.5^\circ$ may mask small-scale climate change information. Therefore, in this study, the cubic spline method [65] was used to interpolate climate data with a spatial resolution of $0.5^\circ \times 0.5^\circ$ and enhance the resolution to $0.25^\circ \times 0.25^\circ$.

Table 1. The primary data and descriptions.

Name	Sources	Resolution	Web Links	Access Date	Format
Digital elevation model	Resource and Environment Science and Data Center	1×1 km	https://www.resdc.cn/data.aspx?DATAID=123	28 September 2019	GRID
1:1 million vegetation map of China	Resource and Environment Science and Data Center	—	https://www.resdc.cn/data.aspx?DATAID=122	1 December 2017	.shp
China's vegetation zoning data	Resource and Environment Science and Data Center	—	http://www.resdc.cn/data.aspx?DATAID=133	1 December 2017	.shp
GIMMS NDVI _{3g}	GIMMS	8×8 km	https://ecocast.arc.nasa.gov/data/pub/GIMMS/	18 November 2018	.nc4
CRU_TS4.02	Climate Research Unit	$0.5^\circ \times 0.5^\circ$	https://crudata.uea.ac.uk/cru/data/hrg/	28 June 2019	.nc

In order to study the temporal and spatial dynamics of climate change in SWC over the past 120 years, we selected the annual average temperature, annual precipitation, seasonal average temperature, and seasonal precipitation as the research indicators to analyze the temporal and spatial changes of the climate in each phase, e.g., in spring (March–May), summer (June–August), autumn (September–November), and winter (December–February).

- (2) The Chinese vegetation zoning data obtained from the Resource and Environmental Science and Data Center reflect the geographical distribution law of Chinese vegetation (see Table 1). Using Arcgis 10.6 software, according to the relevant operation steps (Analysis Tools → Extraction → Clip step), we clipped the vector mapping of the learning area and the vector data consistent with the scope of the learning area were obtained. These mainly included the alpine vegetation area of the tropical monsoon forest and rainforest region, the subtropical evergreen broad-leaved forest region, and the alpine vegetation region of the QX–P, including 13 vegetation zones. The distribution area and location of each vegetation zone were further coordinated and divided into tropical monsoon forest; the east region, northwest region, west-central region, and northwest region of subtropical evergreen broad-leaved forest; and the alpine vegetation region (Figure 1b) [59,60,66].
- (3) The 1:1,000,000 Chinese vegetation atlas obtained from the National Specimen Information Infrastructure (see Table 1) was presented in Arcgis10.6 through the Analysis Tools → Extraction → Clip step; vector data consistent with the range of the learning region were obtained by clipping the vector map of the learning region and obtaining 12 vegetation types (Figure 1c) [59,60,66]. The study area is dominated by forest, shrubs, and grassland (Figure 1c); this comprises about 4/5 of the whole area. In the central and eastern parts of SWC, forest vegetation is the dominant vegetation type, and in the western part of SWC, meadows, grasslands, and shrubs are the dominant vegetation types. Alpine vegetation is also predominantly distributed in the western region, with mostly alpine cushion vegetation and alpine sparse vegetation present [67]. The NDVI value of vegetation gradually decreases from southeast to northwest (Figure 1d) (see Table 1).

2.2.2. Research Methods

- (1) Simple linear regression: Simple linear regression of the climate factors (temperature and precipitation) was performed using the least-squares method on the pixel scale, where the slope of the simple linear regression equation indicated the strength of the climate factor change [44,50]. The formula for the calculation was as follows:

$$k = \frac{n \sum_{i=1}^n ix_i - \sum_{i=1}^n i \sum_{i=1}^n x_i}{n \sum_{i=1}^n i^2 - \left(\sum_{i=1}^n i \right)^2} \quad (1)$$

where n is the length of the research period ($n = 117$ years in this study); x_i is the annual (seasonal) climate factor of the i -th year. When $k > 0$, the climate shows an increasing trend (warming or humidifying) during the study period; conversely, it shows a decreasing trend (cooling or drying) when $k < 0$. Moreover, the significance of the climate factor was checked using a t -test.

- (2) Piecewise linear regression: Using simple linear regression is suitable for masking long time-series trends. Therefore, piecewise linear regression was used in this study, which can intuitively reflect the changing trends of the time series, and related theoretical studies have been widely applied in various fields [44,56,68]. Linear fitting was performed before and after the turning year, and the optimal solution was the turning year with the smallest sum of the squared residuals of the two segments before and after the turning year [56]. The formula was as follows:

$$y = \begin{cases} b_0 + k_1t + \varepsilon & t \leq \alpha \\ b_0 + k_1t + k_2t(t - \alpha) + \varepsilon & t > \alpha \end{cases} \quad (2)$$

where t denotes the year, and y corresponds to the climate change factor for different years. Since α is the transition year of climate factor change, which cannot fully represent the trend in climate change in the short-term, it is stipulated that $1910 \leq \alpha \leq 2008$, that is, no less than 10 years before and after the transition referring to Wang [56]. b_0 , k_1 and k_2 are regression coefficients, and ε represents the residual error.

The significance of the transition year of the climate factor was tested by constructing the F -test, computed as follows:

$$F = \frac{(RSS_{sl} - RSS_{pl})/1}{RSS_{pl}/(n - 3)} \quad (3)$$

where n is the length of samples; RSS_{sl} represents the sum of squared residuals of simple linear regression over the whole period; RSS_{pl} represents the sum of squared residuals when simple linear regression is performed on the two segments before and after the turning year. If the F -values were greater than the critical value of $F_{0.05}(1, n - 3) = 3.924$, this indicated that there were significant turning years at the level of 0.05 in the changes in climate factors.

All data analysis was performed using MATLAB R2019a unless otherwise noted.

3. Results

3.1. Interannual Variation Characteristics of Temperature Factors

3.1.1. Temporal Variation Characteristics of Annual and Seasonal Average Temperatures

The annual and seasonal average temperatures for spring, summer, autumn, and winter over the past 120 years (Figure 2) showed a significant upward trend over the whole period ($p < 0.05$): winter ($0.08 \text{ }^\circ\text{C}/(10 \text{ a})$) > spring ($0.05 \text{ }^\circ\text{C}/(10 \text{ a})$) > annual average ($0.04 \text{ }^\circ\text{C}/(10 \text{ a})$) > autumn ($0.03 \text{ }^\circ\text{C}/(10 \text{ a})$) > summer ($0.03 \text{ }^\circ\text{C}/(10 \text{ a})$); these periods all had obvious segmented characteristics at the significant level of 0.05, with turning years

occurring in 1954, 1948, 1948, 1955, and 1954, respectively. The warming trends before and after the turning years were relatively significant ($p < 0.01$), about 1.60–4.17 times and 2.00–4.84 times the overall rate. Before the turning years, there was a large amplitude in the warming in spring and summer but less warming in winter and autumn, and the opposite was true after the turning year. This suggested that the overall warming rate significantly underestimates the actual warming rate after the 1950s, masking the rapid warming trend before the 1950s, and that the increase in the warming rate over the whole period was mainly caused by the increases in winter and autumn after the turning year.

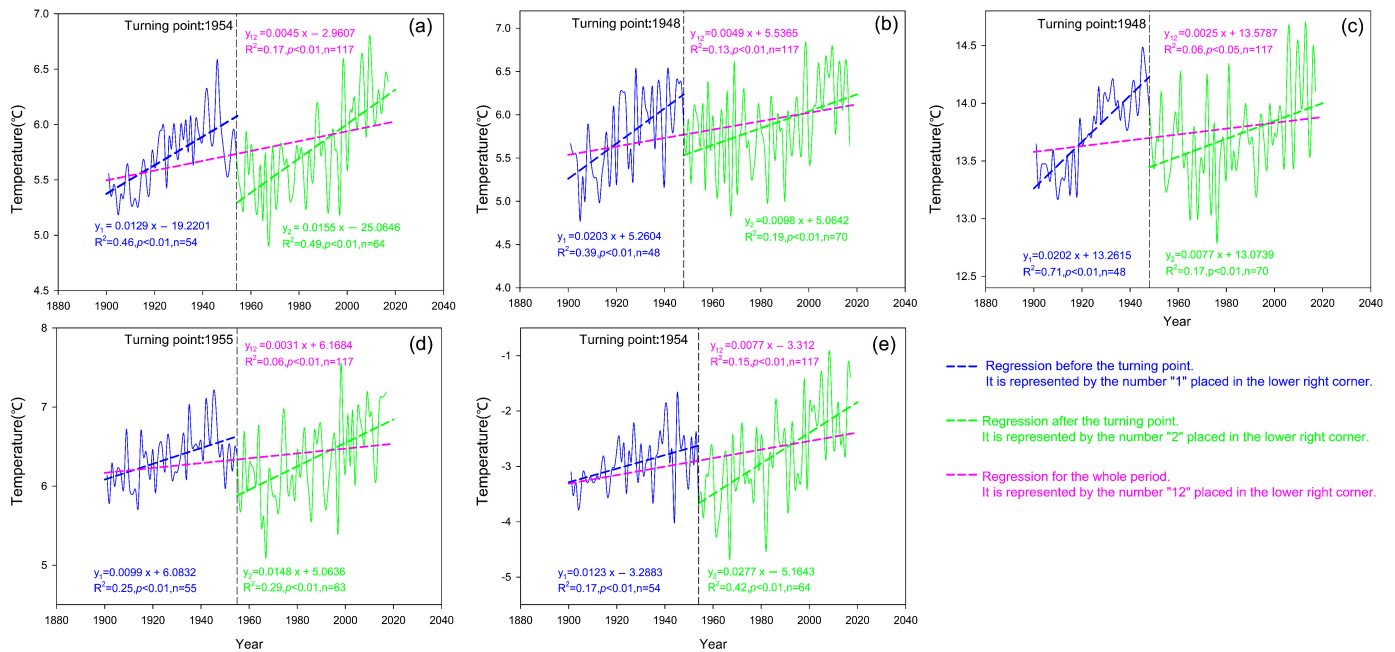


Figure 2. Temporal variation trend of temperature in SWC from 1901 to 2017. (a–e) refer to the annual average, spring, summer, autumn, and winter, respectively. Referring to Wang’s study [56], the turning years were determined via piecewise linear regression equations, and then the regression analysis was performed for the whole period using linear regression equations.

3.1.2. Interannual Spatial Variation Characteristics before and after the Turning Year of Annual and Seasonal Average Temperatures

Interannual Spatial Distribution Characteristics of Turning Years of Annual and Seasonal Average Temperatures

There were significant turning years in the annual and seasonal mean temperature changes in SWC at the grid level, and there were pronounced regional differences in the turning years (Figure 3a–e), which were 1947–1993, 1918–1996, 1921–2005, 1947–1994, and 1948–2001, respectively. Combined with the density diagram (Figure 3f–j), we found that the annual and four seasonal transition years were mainly concentrated in 1947–1965 (97.50%), 1940–1975 (95%), 1947–1973 (94.41%), 1947–1966 (99.65%), and 1948–1962 (87.62%), respectively (the percentages in parentheses indicate the frequency of turning years, which is repeated below). The turning years of the annual average first occurred in the SC–B, most parts of the YG–P, the HD–M, and southeast Xizang, mainly between 1947 and 1950. As time passed, the turning years occurred later, mainly between 1951 and 1955, in the western part of the Southern Qinghai Plateau wide valley, the west of Guoluonaqu hilly plateau, the north of the Eastern Xizang alpine deep valley, and the western regions of the YG–P. The turning years for the scattered distribution in the northwestern part of the Qiangtang Plateau lake basin occurred mainly between 1956 and 1960. Then, the turning years of Kunlun Orogen alpine and plateau, western Qiangtang Plateau lake basin, Southern Xizang Mountains, west of the Eastern Xizang alpine deep valley, and part of the East Himalayas

south limb mainly occurred between 1961 and 1965. In the western part of SWC, the Kunlun Orogen alpine and plateau turning years occurred most recently, concentrated between 1966 and 1993. Similarly, there were patch-like distributions in the turning years of the seasonal average, and the differences were apparent; the peak value and the number of apparent distribution peaks were different.

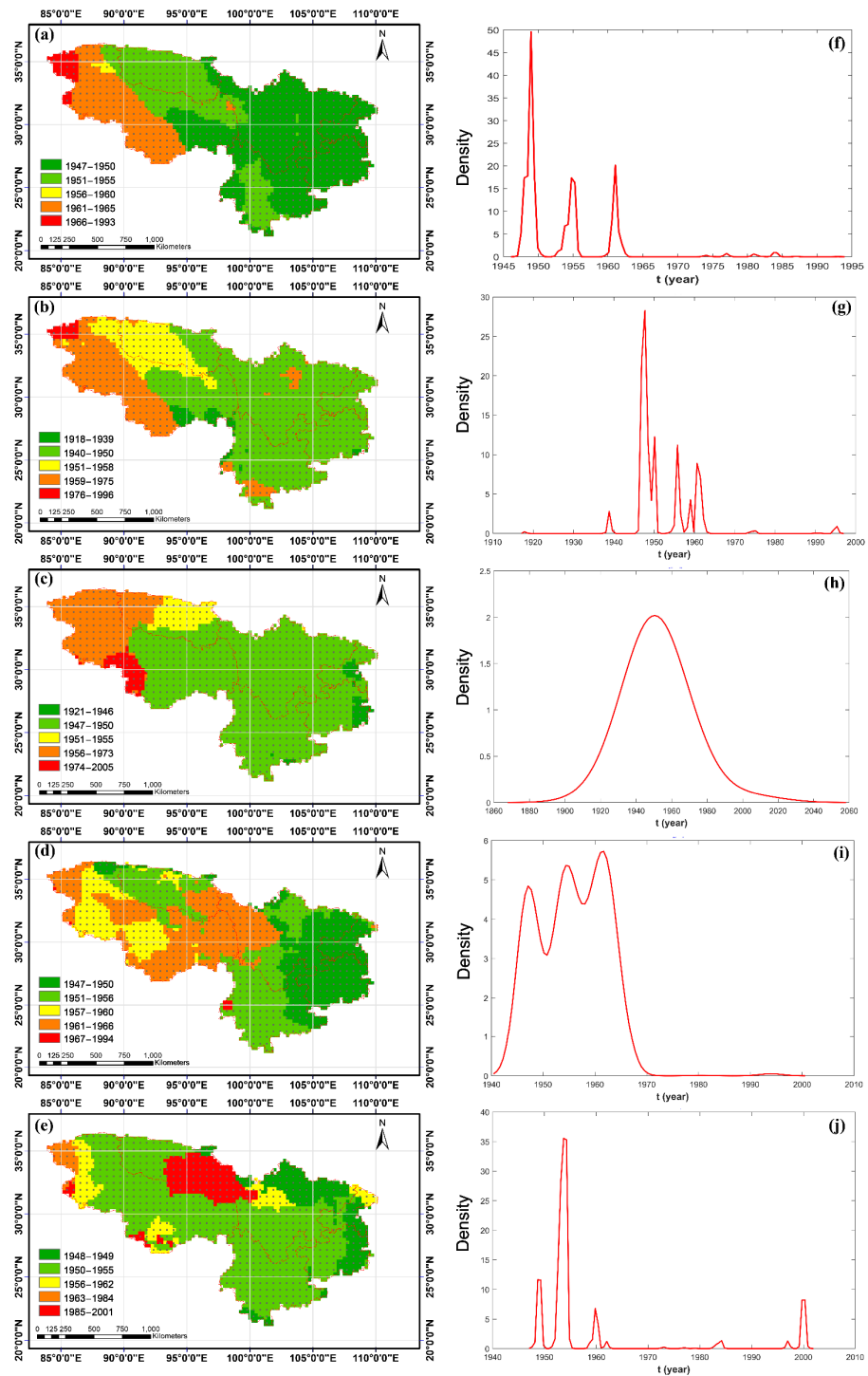


Figure 3. Spatial distribution characteristics of the turning points of annual and seasonal average temperatures in SWC. (a–e) and (f–j) represent the spatial distributions and the density diagrams of turning points referring to the annual average, spring, summer, autumn, and winter, respectively; gray points indicate a significance level of 0.05.

Interannual Spatial Difference Characteristics before and after the Turning Years of Annual and Seasonal Average Temperature

The variation trend of the annual and seasonal average temperature showed a gradually increasing trend from southeast to northwest (Figure 4a₁–e₁), and the regional warming trend was as follows: winter (99.08%) > spring (98.86%) > annual average (98.10%) > autumn (89.79%) > summer (78.21%). The location difference of the temperature increase exceeding 0.05 °C/(10 a) was noticeable, with the annual average temperature mainly occurring in the west of 95° E of SWC. In spring, the difference mainly occurred in the region west of 96° E, the western YG–P, and the northeastern SC–B; in summer, the difference occurred mainly in the northwest of SWC; in autumn, the difference occurred mainly in the west of 93° E; and in winter, the difference occurred mainly in the west of 101° E and the northeastern SC–B. Moreover, the area size of the cooling trend was the largest in summer (22.79%), occurring mainly in the northeastern part of the HD–M, most of the SC–B, and the eastern part of the YG–P, and in Autumn (10.21%), cooling occurred mainly in the northern part of the HD–M and the eastern part of the YG–P. In terms of the annual average, the spring and winter cooling trend areas were very small and less than 2%. It was also found that the significance level of the temperature change trend gradually increased from the middle to the eastern and western ends, and the areas that reached the significance level of 0.05 were mainly concentrated in the western part of SWC and the western part of the YG–P. Before the turning year, the annual and seasonal temperature variability decreased gradually from southeast to northwest, with more than 90% of SWC showing an increasing trend, most of which reached 0.05 significance. After the turning year, the location of the temperature variability shifted significantly, showing a gradual increase from the southeast to the northwest, and again, with more than 90% of the region showing a warming trend.

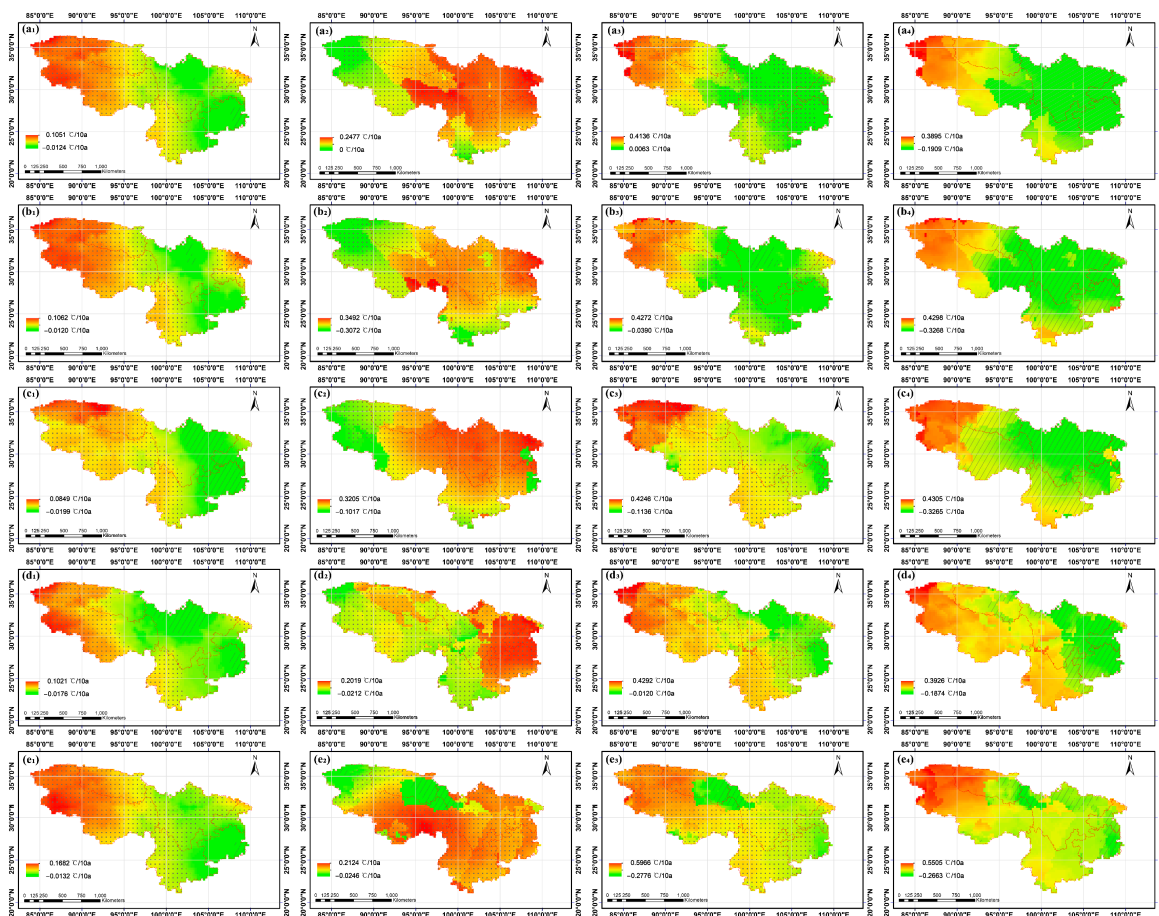


Figure 4. Spatial difference characteristics before and after the turning point of regional annual and

seasonal average temperature in SWC. (a–e) represent the annual average, spring, summer, autumn, and winter, respectively; The number 1 of the lower represents the trend of the whole period; the numbers 2, 3, and 4 of the lower, respectively, represent the changing trends before and after, and the difference before and after the turning year. The gray points represent the significant level of $p < 0.05$, and the shaded diagonal line represents negative values.

The average annual and seasonal warming rates before and after the transition were $0.11\text{ }^{\circ}\text{C}/(10\text{ a})$ to $0.19\text{ }^{\circ}\text{C}/(10\text{ a})$ and $0.10\text{ }^{\circ}\text{C}/(10\text{ a})$ to $0.24\text{ }^{\circ}\text{C}$, which were 1.61–7.09 times and 2.53–3.91 times the value of the overall warming rate, respectively. Before and after the turning year, the warming rate decreased by $0.07\text{ }^{\circ}\text{C}/(10\text{ a})$ and $0.08\text{ }^{\circ}\text{C}/(10\text{ a})$ in spring and summer, and increased by $0.05\text{ }^{\circ}\text{C}/(10\text{ a})$ and $0.12\text{ }^{\circ}\text{C}/(10\text{ a})$ in autumn and winter, respectively, resulting in an increase of $0.0042\text{ }^{\circ}\text{C}/(10\text{ a})$ in the annual average. This suggests that the increase in the mean annual temperature in SWC after the transition year was mainly caused by the increase in winter and autumn warming rates. The regions with reduced/increased warming rates before and after the transition were mainly in the eastern/western parts of SWC, which showed that the spatio-temporal pattern of temperature variability changed significantly before and after the transition, especially in the western part of SWC. In that region, the temperature increases were the most obvious, with the highest values being approximately $0.39\text{ }^{\circ}\text{C}/(10\text{ a})$, $0.43\text{ }^{\circ}\text{C}/(10\text{ a})$, $0.43\text{ }^{\circ}\text{C}/(10\text{ a})$, $0.39\text{ }^{\circ}\text{C}/(10\text{ a})$, and $0.55\text{ }^{\circ}\text{C}/(10\text{ a})$.

3.2. Interannual Variation Characteristics of Precipitation Factors

3.2.1. Temporal Variation Characteristics of Annual and Seasonal Precipitation

Over the past 120 years, the annual and seasonal precipitation has fluctuated considerably (Figure 5), with increasing trends of $0.85\text{ mm}/(10\text{ a})$ and $0.20\text{ mm}/(10\text{ a})$ in spring and winter, respectively, and decreasing trends of $-0.48\text{ mm}/(10\text{ a})$, $-0.24\text{ mm}/(10\text{ a})$, and $-1.30\text{ mm}/(10\text{ a})$ in the annual average, summer, and autumn, respectively, which all had obvious segmented characteristics at the significant level of 0.05, with the turning years occurring in 1928, 1999, 1925, 2002 and 2007, respectively. Before the turning year, the annual average, spring, summer, and winter showed increasing trends, and all but spring reached a significance level of 0.05, with 40.59 times, -94.21 times, and 2.00 times the overall precipitation variability, respectively (the negative sign only indicates that the direction of the precipitation change in the segmented period was inconsistent with the variability in the whole period). After the transition, the annual average, summer, autumn, and winter showed an increasing trend; only the autumn reached a significant increasing trend at the 0.05 level, which was about -18.57 times the overall variability. Before and after the turning years, the variability of spring and summer decreased by $-11.98\text{ mm}/(10\text{ a})$ and $-22.54\text{ mm}/(10\text{ a})$, respectively, while the variability of autumn and winter increased by $25.42\text{ mm}/(10\text{ a})$ and $7.28\text{ mm}/(10\text{ a})$, respectively. Overall precipitation variability at the annual and seasonal levels masked the magnitude and direction of variability around the turning year.

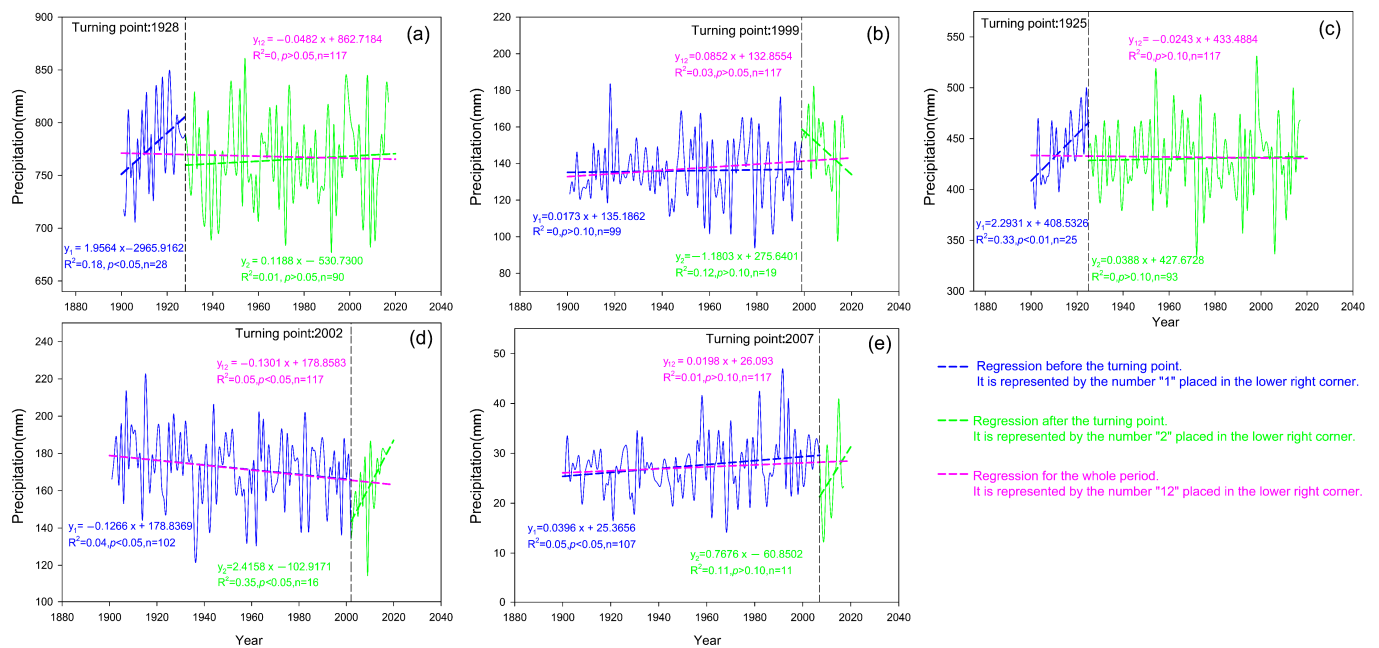


Figure 5. Temporal variation trends of precipitation in SWC from 1901 to 2017. (a–e) refer to the annual average, spring, summer, autumn, and winter, respectively. Referring to Wang’s study [56], the turning years were determined via piecewise linear regression equations, and then regression analysis was performed for the whole period using linear regression equations.

3.2.2. Interannual Spatial Variation Characteristics before and after the Turning Year of Annual and Seasonal Precipitation

Interannual Spatial Distribution Characteristics of Turning Years of Annual and Seasonal Precipitation

The changes in the turning years of annual and seasonal precipitation showed noticeable regional differences in the occurrence time (Figure 6), and more than 92% of the areas reached the significance level of 0.05. Combined with the density map (Figure 3f–j), we found that the turning years of annual and seasonal precipitation were concentrated in the periods 1933–2008 (77.96%), 1953–2000 (79.15%), 1956–2008 (71.06%), 1944–2008 (77.43%), and 1938–2008 (86.07%). The period of the annual turning years spanned about a century (1910 to 2008), with the three earliest patches being in the mid-western part of the YG–P, the eastern part of the SC–B, and the northern part of the HD–M, which occurred between 1910 and 1932. As time passed, there were four smaller patches, which occurred from 1933 to 1946 and were mainly located in the eastern part of the East Himalayas south limb, the northeastern part of the Guoluonaqu hilly plateau, the transition zone from the SC–B to the HD–M, and the eastern part of the YG–P. The regions in which turning occurred from 1947 to 1970 mainly included the western part of the East Himalayas south limb, the connecting area between the Guoluonaqu hilly plateau and the central part of the Eastern Xizang alpine deep valley, and the northwest part of SWC. The regional distribution between 1971 and 1990 was relatively scattered and small, accounting for 6.23% of SWC. The area with the latest transition time mainly has three patches, which are the central and western SC–B and the northeastern YG–P, the western HD–M, and the connecting area of west of 96° E, accounting for 49.67% of SWC. According to the density diagram (Figure 6f), it can be seen that there were two pronounced distribution peaks in the transition year, namely, 1929 (1.51%) and 1998 (2.70%). Similarly, the four seasons had various patch-like distributions of the turning year of precipitation, and the differences were apparent.

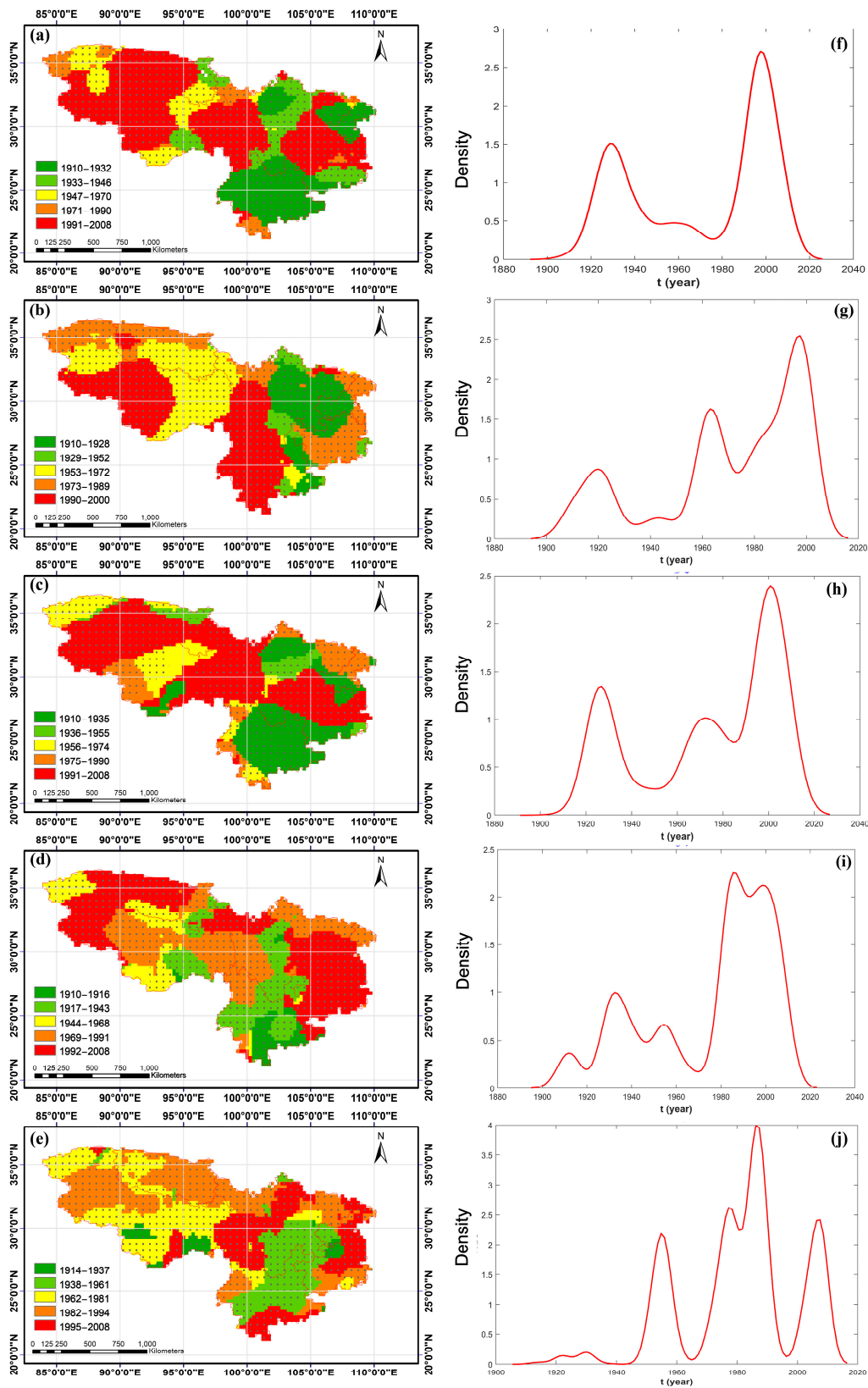


Figure 6. Spatial distribution characteristics of the turning point of annual and seasonal precipitation in SWC. (a–e) and (f–j) represent the spatial distributions and the density diagrams of turning points, referring to the annual average, spring, summer, autumn, and winter, respectively; gray points indicate significance level of 0.05.

Interannual Spatial Difference Characteristics before and after the Turning Years of Annual and Seasonal Precipitation

The trends in the annual average, spring, summer, and autumn gradually increased from southeast to northwest, while winter showed the opposite trend (Figure 7). The increasing trend was as follows: spring (81.83%) > winter (78.33%) > summer (54.03%) > annual average (51.12%) > autumn; where the increase in the annual average occurred in most areas west of 103° E, and the increasing trend of more than 5 mm/(10 a) was mainly in the southwest of the Qiangtang Plateau lake basin and some areas in the Southern Xizang Mountains in the west of SWC. The areas with increased precipitation in spring occurred in most of the areas west of 103° E and the SC–B area. The areas with increased precipitation in summer mainly occurred in the northwestern and southern parts of SWC, and the HD–M, the northern YG–P, and the eastern SC–B. The areas of increased precipitation in autumn occurred mainly in the northwestern portion of SWC. The regions with increased precipitation in winter mainly occurred in most regions north of 30° N and most of the YG–P. The significance levels of the annual average and seasonal precipitation change trends were different, where the significant areas of the annual average were mainly located in the northwest of SWC and scattered in the southern part of southeast Xizang and the central region of the YG–P. In spring, the significant area was the largest (about 49.51%), concentrated in most of the northwestern part of SWC and the HD–M. In summer, the significant areas were concentrated in the Southern Qinghai Plateau wide valley, the northeastern Qiangtang Plateau lake basin, and the East Himalayas south limb. In autumn, the significant areas were concentrated in the southern SC–B and the northern YG–P. In winter, the significant areas were concentrated in the Southern Qinghai Plateau wide valley, the Guoluonaqu hilly plateau in the north, and the HD–M in the north.

Before and after the turning years, apparent location shifts occurred in the regions with decreasing (increasing) precipitation variability and regions with significant precipitation variability. The precipitation variability before and after the turning years reached 1.06–62.78 times and 7.75–37.57 times the overall variability, respectively. Before and after the transition, the precipitation variability decreased by 9.84 mm/(10 a) and 6.13 mm/(10 a) in spring and summer, respectively, and increased by 7.30 mm/(10 a) and 1.97 mm/(10 a) in autumn and winter, respectively, resulting in a decrease of 9.21 mm/(10 a) in the annual average. The decrease in the precipitation variability of the annual average mainly occurred (65.35%) in most of the western part of SWC, the eastern part of the SC–B, most of the YG–P, and the western part of HD–M. The areas with decreased variability in spring (55.61%) mainly occurred in the YG–P, SC–B, and west of 94° E. The areas with decreased variability in summer (61.30%) were concentrated in the central and western YG–P, the eastern SC–B, the western HD–M, the East Himalayas south limb, and northwest of SWC. The areas with decreased variability in autumn (53.90%) were concentrated in the western YG–P, the southern HD–M, and west of 96° E. The areas with decreased variability in winter (67.74%) were mainly located in the western and northeastern YG–P, the mid-west of the SC–B, the western HD–M, and west of SWC. The areas with increased variability before and after the transition were mainly in the western part of the study area in spring and the eastern part of the study area in summer, autumn, and winter. As a result, the annual rate in the northeastern YG–P, the western SC–B, and the northern HD–M showed an increasing trend, and the increase was most evident in the eastern YG–P and the southwestern SC–B, with the highest value reaching 436.89 mm/(10 a).

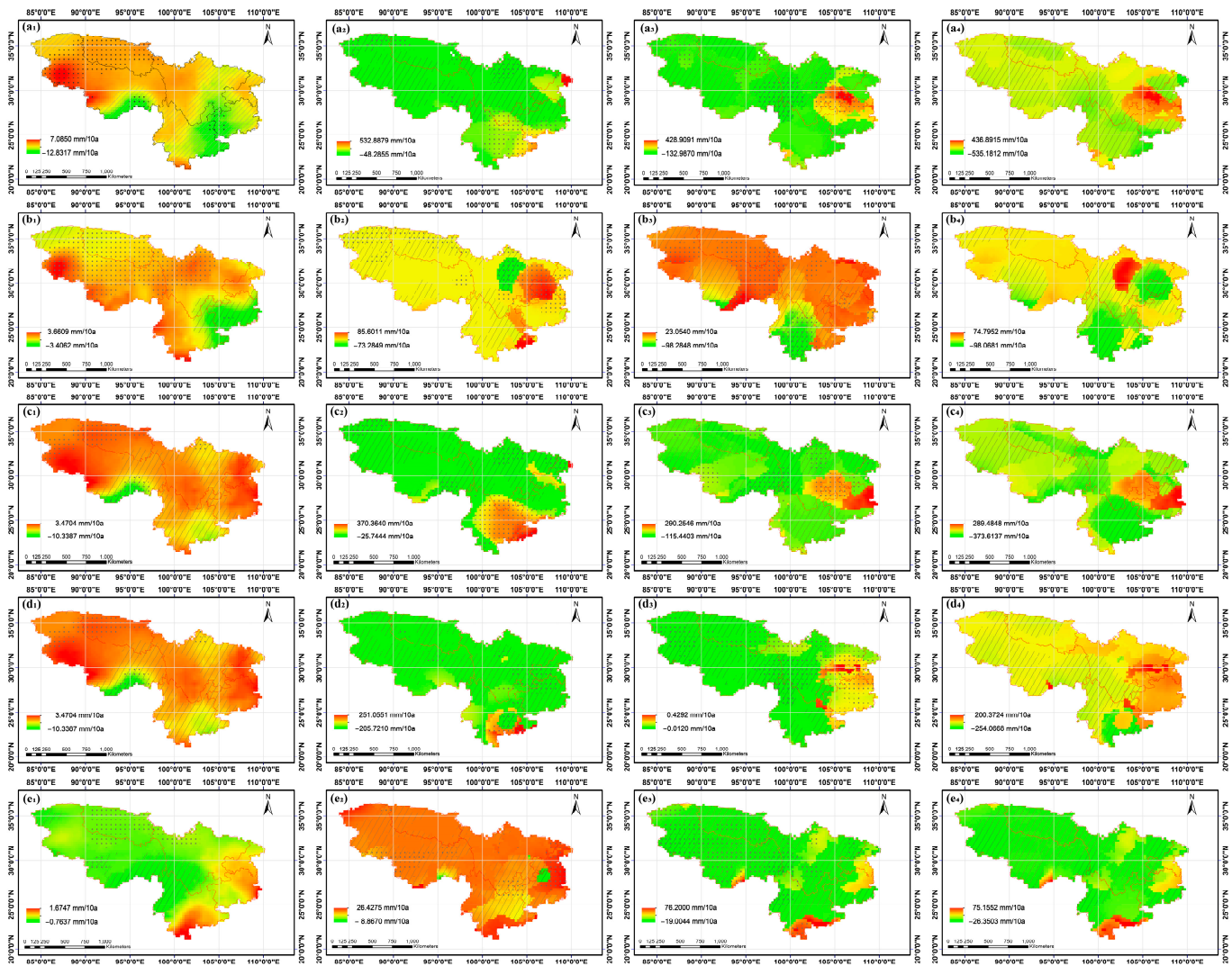


Figure 7. Spatial difference characteristics before and after the turning point of regional annual and seasonal precipitation in SWC. (a–e) represent the annual average, spring, summer, autumn, and winter, respectively. The number 1 of the lower represents the trend over the whole period; the numbers 2, 3, and 4 of the lower, respectively, represent the changing trend before and after, and the difference before and after the turning year. The gray points represent the significance level of $p < 0.05$, and the shaded diagonal line represents negative values.

4. Discussion

4.1. Temporal Variation Characteristics of Climate Change

Numerous studies on climate change have been performed by many scholars at home and abroad, and based on the global datasets HadCRUT5 [13] and NOAA GlobalT [69], global temperature anomalies have increased significantly since the beginning of the twenty-first century relative to the 1850–1900 period, and the warming has a trend of further expansion [1–11]. In this research, the average annual temperature over the past 120 years showed a significant increasing trend, reaching $0.04\text{ }^{\circ}\text{C}/(10\text{ a})$ ($p < 0.01$), which was lower than the rate of global land temperature increase ($1.00 \pm 0.06\text{ }^{\circ}\text{C}/(100\text{ a})$) estimated by Xu et al. [5] and Yun et al. [7]. Further, the *F*-test showed that there was an obvious turning year in 1954, and the warming rate reached $0.13\text{ }^{\circ}\text{C}/(10\text{ a})$ ($p < 0.01$) and $0.16\text{ }^{\circ}\text{C}/(10\text{ a})$ ($p < 0.01$) before and after the turning year, respectively, exceeding the global land temperature growth trend. However, the growth rate after the turning year was about 3.44 times that of the whole period, which generally agrees with the results of other scholars [54]. Combined with Wang’s study [59], the average trend rate of temperature

from 1982 to 2017 was also analyzed in this region, with a result of $0.26\text{ }^{\circ}\text{C}/(10)$, indicating that the warming rate had been increasing over the past 30 years, and there was no interruption (slowing down or stagnation) of global warming [70,71]. The beginning of the warming in this study was significantly earlier than that reported by other scholars; the temperature of the QX–P began to increase gradually in the 1960s [9,34,72], and that of the Northern Hemisphere started to increase in the mid-1970s [13,54,73] and continued to increase, especially after 1980 [9,13,14,73,74]. Several studies have detailed the study period, such as the global surface temperature trend from 1901 to 1940, as the first warm period, with 1941 to 1970 as the cooling period, and 1971 to 2014 as the fast warming period [16]. However, the annual precipitation fluctuated greatly, showing a decreasing trend ($-0.48\text{ mm}/(10\text{ a})$, $p > 0.05$) and a weak increasing trend after the turning year (1928) ($1.19\text{ mm}/(10\text{ a})$, $p > 0.05$). Wang [59] also analyzed the average tendency rate of the annual precipitation change trend in the study area from 1982 to 2017, which was $6.37\text{ mm}/(10)$, indicating that the annual precipitation change fluctuated greatly, and the differences in each period were different. Duan [14] and Li [75] observed that the precipitation on the QX–P had gradually increased since the 1960s; this was delayed compared with the outcomes of this research. Furthermore, the outcomes of analyzing trends in observations over one period cannot simply be applied to another, and climate change varies over time [76–78]. Sun et al.'s [78] analysis with the CMST-Interim dataset confirmed that the global warming trend has further expanded since 1950, and the average temperature increases between 1900 and 2018 and 1950 and 2018 were $0.089 \pm 0.004\text{ }^{\circ}\text{C}/(10\text{ a})$ and $0.137 \pm 0.007\text{ }^{\circ}\text{C}/(10\text{ a})$, respectively. Oguntunde et al. [76] found an increasing trend in Nigeria from 1931 to 1960 and a rapid decrease between 1961 and 1990. Li et al. [77] observed that global arid areas' dry/wet patterns in the past 60 years exhibited significant differences before and after 1980, and the dry land of the American (African) continent showed a wet trend from 1948 to 1979 and a dry (slightly wet) trend from 1980 to 2008. Other researchers (e.g., Greve et al. [29]; Vicente-Serrano et al. [30]; Dai [27]) found that since 1950, precipitation has increased in central and high latitudes of Eurasia, southeastern South America, the central United States, and northwestern Australia, while the opposite trend has been observed over much of Africa, southern Europe, East Asia, South Asia, the Mediterranean, and high latitudes.

4.2. Spatial Variation Characteristics of Climate Change

In this research, the annual average state of the annual average temperature and precipitation over the past 120 years has shown a gradually decreasing tendency from southeast to northwest, and the corresponding change trend was gradually increasing, while the well-known paradigm of “dry to dry and wet to wet, cold to cold and hot to hot” did not occur. The main reason is that dry regions become drier and wet regions become wetter only when the deviations in both precipitation and evaporation are considered [29,79]. The altitude of SWC successively rises from the southeast to the northwest, the sensitivity to global climate change gradually increases, and there is an elevation-dependent warming phenomenon [24,49,50,58]. At the same time, the vegetation NDVI has gradually decreased (Figure 1d), and the effect of reducing the local temperature gradually decreased through the biophysical feedback of vegetation [44,45,47,48,80], without the paradigm of “cold becomes cold and hot becomes hot”. In general, about 78.33% of the Qinghai–Xizang region west of 98° E in SWC has experienced the process of warming and wetting, which is consistent with the rule that most researchers report that the Qinghai–Xizang region has experienced rapid warming and warming on the whole based on station data [1,9,11,74,81]. This may be related to the changes in atmospheric dynamic and thermal structure, including the increase in the sea-surface temperature, the northward shift of westerlies, the warming trend of the middle and upper troposphere, and the occurrence frequency of low-level vortices on the ground [82–89]. In recent decades, the circulation trend over the troposphere of Asia has been increasing, with the influence of low-latitude westerlies increasing, and more water vapor being transported from the Arabian Sea, resulting in increased precipitation variability [86–89]. Some studies also point to warming in the southwestern Pacific Ocean

and the central Indian Ocean as a major cause of warming-wetting on the QX–P [82]. In addition, Zhang et al. [90] and Curio et al. [91] found that precipitation on the QX–P and its surrounding areas largely depends on cyclic processes related to regional evaporation and that increased temperature variability accelerates glacier melting, further leading to more evaporation, promoting local water cycling and increasing local atmospheric water vapor content. Increasing temperature and decreasing dew point increase the condensation level, gradually increasing regional precipitation variability [53,92,93]. Global warming will likely play a more critical role in regulating precipitation over the QX–P. However, in the eastern part of SWC, the trend was primarily (about 68.52%) warm and dry, which was similar to the results reported by the China Meteorological Administration [9], Yang [81], and the IPCC [1]. These results suggest that the East and South Asian monsoon (Indian Summer Monsoon) have been shrinking, bringing less water vapor and leading to less precipitation in this part of the region in recent decades [94,95].

At the spatial level, the turning years of inter-annual and seasonal mean temperature were gradually delayed from east to west, mainly concentrated in the period 1940–1975 (about 95%), and reached the significance level of 0.05 before the turning year, showing a decreasing trend from southeast to northwest, and after the turning year, an increasing trend. In addition, the warming rate increased by $0.04\text{ }^{\circ}\text{C}/(10\text{ a})$ before and after the transition on the inter-annual scale, indicating that the warming rate continued to increase continuously over time, which agrees with the results obtained by most researchers at the global level, and for the Northern Hemisphere and the QX–P; the global climate is experiencing significant warming and continues to accelerate with time [1,2,5,7,9,10,13,34]. After the turning years, significant areas decreased in spring, summer, and autumn but increased in winter. Moreover, the warming rate in spring and summer decreased by $0.07\text{ }^{\circ}\text{C}/(10\text{ a})$ and $0.08\text{ }^{\circ}\text{C}/(10\text{ a})$, and increased in autumn and winter by $0.05\text{ }^{\circ}\text{C}/(10\text{ a})$ and $0.12\text{ }^{\circ}\text{C}/(10\text{ a})$, respectively, which further indicates the increase in annual average temperature after the transition. This is primarily attributed to the increase during winter and autumn, and agrees with the outcomes obtained by Liu et al. [96] and Wang et al. [97]. For example, Liu et al. [96] revealed that the QX–P experienced significant warming, and the warming peaks in the monthly maximum, minimum, and mean values occurred in winter from 1971 to 2015. Wang et al. [97] observed that the highest warming rate of the southern Xizang Plateau from 1961 to 2012 also occurred in winter. This may be due to differences in cloud cover over the surface, with higher cloud cover in the lower layers during the summer and spring, especially during the summer, when convective cloud systems are more developed [98] and the water vapor contained in the lower clouds has a higher albedo. At this time, under lower cloud height and more extensive cloud cover, the top of the cloud layer is heated, preventing clouds from absorbing more long-wave radiation, so the cloud layer has a chilling effect on the atmosphere at the bottom of the surface cloud. However, in winter, the cloud cover was lower, and the temperature rose faster, which made a more significant contribution to interannual warming [99].

The warming rate was more significant in the west after the site turning year, which may be due to the increased temperature promoting vegetation growth. In particular, the eastern part of SWC is distributed in the central subtropical and south subtropical humid regions (Figure 1b), which have a more pronounced boosting effect on vegetation growth. Vegetation coverage increases and albedo decreases (Figure 1d) affect thermal convection or surface evapotranspiration, and reducing the local surface temperature will mitigate climate change and further regulate local climate change [44,47,48,80,100]. Shen et al. [100] reported that the QX–P has been continuously warming, and vegetation activities have been continuously enhanced over the past three decades, resulting in enhanced local transpiration, reduced surface energy, and reduced local mean temperature during the growing season. According to the fifth report of the IPCC [1], increasing vegetation cover can alleviate the temperature in some areas. The vegetation coverage in SWC was calculated by referring to Pei et al. [101], where the vegetation coverage in the western part of SWC was low (generally less than 30%). The vegetation type is dominated by steppe, grass–forb

community, and meadow (see Table 1), where the relatively small amount of surface soil moisture results in low transpiration, with more heat being released at night. In other words, the strong albedo may mask the cooling effect of evapotranspiration, resulting in a significant warming rate in this region [47,48].

The vegetation coverage in the eastern SWC is relatively extensive, mostly more than 60% (see Table 1), and is dominated by vegetation types such as needleleaf forest, broadleaf forest, and scrub. The corresponding surface albedo is relatively low and belongs to the humid region, with the soil moisture being relatively high on the underlying surface of the vegetation layer, and the evaporation being relatively strong, which reduces the temperature in this part of the region. In addition, it increases the water vapor content over the regional surface, which is conducive to the formation of clouds, further reducing the solar radiation and lowering the temperature [45,80,102], which can offset or partially offset the global warming and even trigger a cooling trend (such as in the eastern YG–P in Figure 4a₁). Several studies have also shown that the proximity of the QX–P to the two major light-absorbing aerosol-emitting regions in East and South Asia significantly reduces the ice/snow albedo and contributes to atmospheric warming [103]. The rapid ozone depletion has led to tropospheric warming on the QX–P [104], and snow albedo feedback with increasing topographic height has also contributed to warming [105]. Recent studies have also shown that anthropogenic driving and the increase in greenhouse gases were the dominant factors in the rapid warming stage of the QX–P [106], and the contribution rate of anthropogenic heat warming in most areas of the plateau was more than 50%. For example, as the Southwest entered a period of peaceful development in the 1950s, the population gradually increased, especially due to the development of the western region in China, which raised people's living standards, produced more greenhouse gas emissions, and increased the warming rate.

4.3. Limitations of the Present Analysis

Although CRU data have been successfully applied to climate change analysis on global and regional scales [44,59,63,64], due to environmental factors such as the complex terrain in SWC, the observation points of meteorological stations in the study area were minimal. In particular, the conventional observation points on the QX–P were minimal, such as Qinghai (only seven stations) and Tibet (only 28 stations), and most of the remaining points were located in the eastern and peripheral areas of the study area [106,107]. The spatial distribution of meteorological stations did not follow the rules of discrete distribution, being far lower than the minimum allowable station density recommended by the World Meteorological Organization (40–100 stations per $10^4 \cdot \text{km}^2$) in temperate and tropical humid mountainous areas. This may increase the uncertainty in presenting the results for the continuous spatial distribution of water and heat in the study area, so that the inadequacy of routine observations also affects the accuracy of the reanalyzed data, resulting in more significant uncertainty than elsewhere [106–108]. Only the average value on the annual and seasonal scales was analyzed, and the pattern of climate change should be further analyzed by combining the maximum and minimum values. At present, in order to intuitively analyze the situation of the turning year, we only analyzed the situation of one turning year on the grid scale, while there might be multiple transition points in actual climate change series. We also tested the trends using the M–K and *t*-test methods and found that there are several transition periods in the annual mean temperature, such as the abrupt changes in 1918–1921, 1947–1952, and 1997–2002. Next, we will continue to deeply analyze the variation trends and jump-point characteristics of time series of climatic factors.

5. Conclusions

Overall, we have shown that the variation in temperature and precipitation factors has a distinct segmented character, with significant turning years with distinct regional and phase characteristics in SWC over the past 120 years. The annual (seasonal) climate change has prominent segmented characteristics; in terms of time, there were significant turning

years in 1954 for temperature and 1928 for precipitation, and the overall temporal variability obscured the magnitude or direction of the variability before and after the turnaround year. Regarding space, the significant turning years were concentrated in the periods 1940–1993 (temperature) and 1910–2008 (precipitation), and the climate factor variability before and after the turning years exhibited a pronounced location shift. Furthermore, the comprehensive analysis of the inter-annual and inter-seasonal variability rates of climate factors further revealed an increasing trend of climate factor variability after the turning years, which was mainly caused by an increase in winter and autumn variability. Therefore, more attention should be paid to clarifying the distribution of study periods and regions when analyzing climate change trends. To the extent that this research provided a necessary theoretical basis for effectively revealing the spatio-temporal variability properties of climate factors against the background of global climate change, more attention should be paid to the location and phase of the study.

Author Contributions: Conceptualization, M.W.; methodology, M.W. and S.W.; software, M.W. and S.W.; validation, M.W. and Z.A.; formal analysis, M.W. and S.W.; investigation, M.W.; resources, M.W.; data curation, M.W.; writing—original draft preparation, M.W. and Z.A.; writing—review and editing, M.W. and Z.A.; visualization, M.W.; supervision, M.W.; project administration, M.W.; funding acquisition, M.W. All authors have read and agreed to the published version of the manuscript.

Funding: This research was funded by Chaozhou Special Fund for Human Resource Development, grant number 2023.

Institutional Review Board Statement: Not applicable.

Informed Consent Statement: Not applicable.

Data Availability Statement: The climate data (CRU_TS4.02) were obtained from <https://crudata.uea.ac.uk/cru/data/hrg/>, accessed on 18 December 2018.

Conflicts of Interest: The authors declare no conflict of interest.

References

1. IPCC. *Climate Change 2013: The Physical Science Basis: Summary for Policymakers*; Cambridge University Press: Cambridge, UK, 2013.
2. IPCC. *Special Report on Global Warming of 1.5 °C*; Cambridge University Press: Cambridge, UK, 2018.
3. IPCC. *Climate Change 2021: The Physical Science Basis*. In *Contribution of Working Group I to the Sixth Assessment Report of the Intergovernmental Panel on Climate Change*; Cambridge University Press: Cambridge, UK, 2021.
4. Marotzke, J.; Forster, P.M. Forcing, feedback and internal variability in global temperature trends. *Nature* **2015**, *517*, 565–570. [[CrossRef](#)]
5. Xu, Y.Y.; Ramanathan, V.; Victor, D.G. Global warming will happen faster than we think. *Nature* **2018**, *564*, 30–32. [[CrossRef](#)] [[PubMed](#)]
6. Gollledge, N.R.; Keller, E.D.; Gomez, N.; Naughten, K.A.; Bernales, J.; Trusel, L.D.; Edwards, T.L. Global environmental consequences of twenty-first-century ice-sheet melt. *Nature* **2019**, *566*, 65–72. [[CrossRef](#)]
7. Yun, X.; Huang, B.Y.; Cheng, J.Y.; Xu, W.H.; Qiao, S.B.; Li, Q.X. A new merge of global surface temperature datasets since the start of 20th century. *Earth Syst. Sci. Data* **2019**, *11*, 1629–1643. [[CrossRef](#)]
8. Bell, R.E.; Seroussi, H. History, mass loss, structure, and dynamic behavior of the Antarctic Ice Sheet. *Science* **2020**, *367*, 1321–1325. [[CrossRef](#)]
9. China Meteorological Administration. *Blue Book on Climate Change in China 2020*; Science Press: Beijing, China, 2020.
10. China Meteorological Administration. *Blue Book on Climate Change in China 2022*; Science Press: Beijing, China, 2022.
11. Zhao, W.J. Extreme weather and climate events in China under changing climate. *Natl. Sci. Rev.* **2020**, *7*, 938–943. [[CrossRef](#)]
12. IPCC. Emergent risks and key vulnerabilities. In *Climate Change 2014: Impacts, Adaptation, and Vulnerability. Part A: Global and Sectoral Aspects. Contribution of Working Group II to the Fifth Assessment Report of the Intergovernmental Panel on Climate Change*. Intergovernmental Panel on Climate Change; Field, C.B., Barros, V.R., Dokken, D.J., Mach, K.J., Mastrandrea, M.D., Bilir, T.E., Chatterjee, M., Ebi, K.L., Estrada, Y.O., Genova, R.C., et al., Eds.; Cambridge University Press: Cambridge, UK, 2014.
13. Morice, C.P.; Kennedy, J.J.; Rayner, N.A.; Winn, J.P.; Hogan, E.; Killick, R.E.; Dunn, R.J.H.; Osborn, T.J.; Jones, P.D.; Simpson, I.R. An updated assessment of near-surface temperature change from 1850: The HadCRUT5 dataset. *J. Geophys. Res. Atmos.* **2021**, *126*, e2019JD032361. [[CrossRef](#)]
14. Duan, J.P.; Li, L.; Chen, L.; Zhang, H.X. Time-dependent warming amplification over the Tibetan Plateau during the past few decades. *Atmos. Sci. Lett.* **2020**, *21*, e998. [[CrossRef](#)]

15. Feng, S.; Hu, Q.; Huang, W.; Ho, C.H.; Li, R.; Tang, Z. Projected climate regime shift under future global warming from multi-model, multi-scenario CMIP5 simulations. *Glob. Planet. Chang.* **2014**, *112*, 41–52. [[CrossRef](#)]
16. Fan, X.W.; Duan, Q.Y.; Shen, C.W.; Wu, Y.; Xing, C. Global surface air temperatures in CMIP6: Historical performance and future changes. *Environ. Res. Lett.* **2020**, *15*, 104056. [[CrossRef](#)]
17. Flynn, C.M.; Mauritsen, T. On the climate sensitivity and historical warming evolution in recent coupled model ensembles. *Atmos. Chem. Phys.* **2020**, *20*, 7829–7842. [[CrossRef](#)]
18. Gillett, N.P.; Kirchmeier-Young, M.; Ribes, A.; Wu, T.W.; Yukimoto, S.; Ziehn, T. Constraining human contributions to observed warming since the pre-industrial period. *Nat. Clim. Chang.* **2021**, *11*, 207–212. [[CrossRef](#)]
19. Zhao, P.; Jones, P.; Cao, L.J.; Yan, Z.W.; Zha, S.Y.; Zhu, Y.N.; Yu, Y.; Tang, G.L. Trend of surface air temperature in eastern China and associated large-scale climate variability over the last 100 years. *J. Clim.* **2014**, *27*, 4693–4703. [[CrossRef](#)]
20. Wang, J.F.; Xu, C.D.; Hu, M.G.; Li, Q.X.; Yan, Z.W.; Jones, P. Global land surface air temperature dynamics since 1880. *Int. J. Climatol.* **2018**, *38*, e466–e474. [[CrossRef](#)]
21. Zhou, C.; Wang, K. Land surface temperature over global deserts: Means, variability, and trends. *J. Geophys. Res. Atmos.* **2016**, *121*, 14344–14357. [[CrossRef](#)]
22. Retamales-Muñoz, G.; Durán-Alarcón, C.; Mattar, C. Recent land surface temperature patterns in Antarctica using satellite and reanalysis data. *J. South. Am. Earth. Sci.* **2019**, *95*, 102304. [[CrossRef](#)]
23. Liu, J.; Hagan, F.T.; Liu, Y. Global Land Surface Temperature Change (2003–2017) and Its Relationship with Climate Drivers: AIRS, MODIS, and ERA5-Land Based Analysis. *Remote Sens.* **2021**, *13*, 44. [[CrossRef](#)]
24. Li, B.F.; Chen, Y.N.; Shi, X. Does elevation dependent warming exist in high mountain Asia? *Environ. Res. Lett.* **2020**, *15*, 024012. [[CrossRef](#)]
25. Jaber, S.M.; Abu-Allaban, M.M. TRMM 3B43 Product-Based Spatial and Temporal Anatomy of Precipitation Trends: Global Perspective. *Environ. Monit. Assess.* **2020**, *192*, 437. [[CrossRef](#)]
26. Zeng, Z.; Li, Y.; Wu, W.; Zhou, Y.; Wang, X.; Huang, H.; Li, Z. Spatio-Temporal Variation of Drought within the Vegetation Growing Season in North Hemisphere (1982–2015). *Water* **2020**, *12*, 2146. [[CrossRef](#)]
27. Dai, A. Hydroclimatic trends during 1950–2018 over global land. *Clim. Dyn.* **2021**, *56*, 4027–4049. [[CrossRef](#)]
28. Nguyen, P.; Thorstensen, A.; Sorooshian, S.; Hsu, K.; Aghakouchak, A.; Ashouri, H.; Tran, H.; Braithwaite, D. Global precipitation trends across spatial scales using satellite observations. *Bull. Am. Meteorol. Soc.* **2018**, *99*, 689–697. [[CrossRef](#)]
29. Greve, P.; Orłowsky, B.; Mueller, B.; Sheffield, J.; Reichstein, M.; Seneviratne, S.I. Global assessment of trends in wetting and drying over land. *Nat. Geosci.* **2014**, *7*, 716–721. [[CrossRef](#)]
30. Vicente-Serrano, S.M.; Quiring, S.; Peña-Gallardo, M.; Domínguez-castro, F.; Yuan, S. A review of environmental droughts: Increased risk under global warming? *Earth. Sci. Rev.* **2020**, *201*, 102953. [[CrossRef](#)]
31. Yan, Z.W.; Ding, Y.H.; Zhai, P.M.; Song, L.C.; Cao, L.J.; Li, Z. Re-assessing climatic warming in China since the last century. *Acta Meteor. Sinica* **2020**, *78*, 370–378. (In Chinese)
32. Jin, K.; Wang, F.; Yu, Q.; Gou, J.J.; Liu, H.H. Varied degrees of urbanization effects on observed surface air temperature trends in China. *Clim. Res.* **2018**, *76*, 131–143. [[CrossRef](#)]
33. Cao, L.; Zhu, Y.; Tang, G.; Yuan, F.; Yan, Z. Climatic warming in China according to a homogenized data set from 2419 stations. *Int. J. Climatol.* **2016**, *36*, 4384–4392. [[CrossRef](#)]
34. Piao, S.L.; Ciais, P.; Huang, Y.; Yu, Y.Q.; Zhang, T.Y.; Fang, J.Y. The impacts of climate change on water resources and agriculture in China. *Nature* **2010**, *467*, 43–51. [[CrossRef](#)]
35. Ding, Y.H. *Climate Change and Prediction in China*; China Meteorological Press: Beijing, China, 2016. (In Chinese)
36. Tan, X.; Wu, Y.; Liu, B.; Chen, S. Inconsistent changes in global precipitation seasonality in seven precipitation datasets. *Clim. Dyn.* **2020**, *54*, 3091–3108. [[CrossRef](#)]
37. Ma, S.M.; Zhou, T.J.; Dai, A.G.; Han, Z.Y. Observed changes in the distributions of daily precipitation frequency and amount over China from 1960 to 2013. *J. Clim.* **2015**, *28*, 6960–6978. [[CrossRef](#)]
38. Köppen, W. Die Wärmazonen der Erde, nach der Dauer der heissen, gemässigten, und kalten Zeit und nach der Wirkung der Wärme auf die organische Welt betrachtet. *Meteorol. Z.* **1884**, *1*, 215–226.
39. Guan, Y.L.; Lu, H.W.; Yin, C.; Xue, Y.X.; Jiang, Y.L.; Kang, Y.; He, L.; Heiskanen, J. Vegetation response to climate zone dynamics and its impacts on surface soil water content and albedo in China. *Sci. Total. Environ.* **2020**, *747*, 141537. [[CrossRef](#)] [[PubMed](#)]
40. Guan, Y.L.; Lu, H.W.; He, L.; Adhikari, H.; Pellikka, P.; Maeda, E.; Heiskanen, J. Intensification of the dispersion of the global climatic landscape and its potential as a new climate change indicator. *Environ. Res. Lett.* **2020**, *15*, 114032. [[CrossRef](#)]
41. Beck, H.E.; Zimmermann, N.E.; McVicar, T.R.; Vergopolan, N.; Berg, A.; Wood, E.F. Present and future Köppen-Geiger climate classification maps at 1-km resolution. *Sci. Data* **2018**, *5*, 180214. [[CrossRef](#)] [[PubMed](#)]
42. Garcia, R.A.; Cabeza, M.; Rahbek, C.; Araújo, M.B. Multiple dimensions of climate change and their implications for biodiversity. *Science* **2014**, *344*, 1247579. [[CrossRef](#)]
43. Chan, D.; Wu, Q. Significant anthropogenic-induced changes of climate classes since 1950. *Sci. Rep.* **2015**, *5*, 13487. [[CrossRef](#)] [[PubMed](#)]
44. Wang, M.; Jiang, C.; Sun, O.J. Spatially differentiated changes in regional climate and underlying drivers in southwestern China. *J. For. Res.* **2022**, *33*, 755–765. [[CrossRef](#)]

45. Zeng, Z.Z.; Piao, S.L.; Li, L.Z.X.; Zhou, L.M.; Ciais, P.; Wang, T.; Li, Y.; Lian, X.; Wood, E.F.; Friedlingstein, P.; et al. Climate mitigation from vegetation biophysical feedbacks during the past three decades. *Nat. Clim. Chang.* **2017**, *7*, 432–436. [[CrossRef](#)]
46. Alkama, R.; Cescatti, A. Climate change: Biophysical climate impacts of recent changes in global forest cover. *Science* **2016**, *351*, 600–604. [[CrossRef](#)]
47. Huang, B.; Hu, X.P.; Fuglstad, G.A.; Zhou, X.; Zhao, W.W.; Cherubini, F. Predominant regional biophysical cooling from recent land cover changes in Europe. *Nat. Commun.* **2020**, *11*, 1066. [[CrossRef](#)]
48. Peng, S.S.; Piao, S.L.; Zeng, Z.Z.; Ciais, P.; Zhou, L.M.; Li, L.Z.X.; Myneni, R.B.; Yin, Y.; Zeng, H. Afforestation in China cools local land surface temperature. *Proc. Natl. Acad. Sci. USA* **2014**, *111*, 2915–2919. [[CrossRef](#)] [[PubMed](#)]
49. Pepin, N.; Bradley, R.S.; Diaz, H.F.; Baraer, M.; Caceres, E.B.; Forsythe, N.; Fowler, H.; Greenwood, G.; Hashmi, M.Z.; Liu, X.D.; et al. Elevation-dependent warming in mountain regions of the world. *Nat. Clim. Chang.* **2015**, *5*, 424–430.
50. Li, X.P.; Wang, L.; Guo, X.Y.; Chen, D.L. Does summer precipitation trend over and around the Tibetan Plateau depend on elevation? *Int. J. Climatol.* **2017**, *37*, 1278–1284. [[CrossRef](#)]
51. Aguilar-Lome, J.; Espinoza-Villar, R.; Espinoza, J.C.; Rojas-Acuña, J.; Willems, B.L.; Leyva-Molina, W.M. Elevation-dependent warming of land surface temperatures in the Andes assessed using MODIS LST time series (2000–2017). *Int. J. Appl. Earth. Obs.* **2019**, *77*, 119–128. [[CrossRef](#)]
52. Fan, Z.X.; Bräuning, A.; Thomas, A.; Li, J.B.; Cao, K.F. Spatial and temporal temperature trends on the Yunnan Plateau (Southwest China) during 1961–2004. *Int. J. Climatol.* **2011**, *31*, 2078–2090. [[CrossRef](#)]
53. Palazzi, E.; Mortarini, L.; Terzago, S.; von Hardenberg, J. Elevation-dependent warming in global climate model simulations at high spatial resolution. *Clim. Dyn.* **2019**, *52*, 2685–2702. [[CrossRef](#)]
54. Kang, S.C.; Xu, Y.W.; You, Q.L.; Flugel, W.A.; Pepin, N.; Yao, T.D. Review of climate and cryospheric change in the Tibetan Plateau. *Environ. Res. Lett.* **2010**, *5*, 015101. [[CrossRef](#)]
55. Guo, D.; Sun, J.; Yang, K.; Pepin, N.; Xu, Y. Revisiting Recent Elevation-Dependent Warming on the Tibetan Plateau Using Satellite-Based Data Sets. *J. Geophys. Res. Atmos.* **2019**, *124*, 8511–8521. [[CrossRef](#)]
56. Wang, S.P.; Wang, Z.H.; Piao, S.L.; Fang, J.Y. Regional differences in the timing of recent air warming during the past four decades in China. *Chin. Sci. Bull.* **2010**, *55*, 1968–1973. [[CrossRef](#)]
57. Li, X.C. *Historical Geography: Geopolitics, Regional Economy and Culture*; Peking University Press: Beijing, China, 2004; pp. 79–93. (In Chinese)
58. You, Q.; Chen, D.; Wu, F.; Pepin, N.; Cai, Z.; Ahrens, B.; Jiang, Z.; Wu, Z.; Kang, S.; Amir, A.K. Elevation dependent warming over the Tibetan Plateau: Patterns, mechanisms and perspectives. *Earth-Sci. Rev.* **2020**, *210*, 103349. [[CrossRef](#)]
59. Wang, M.; An, Z. Regional and Phased Vegetation Responses to Climate Change Are Different in Southwest China. *Land* **2022**, *11*, 1179. [[CrossRef](#)]
60. Wang, M.; An, Z.; Wang, S. The Time Lag Effect Improves Prediction of the Effects of Climate Change on Vegetation Growth in Southwest China. *Remote Sens.* **2022**, *14*, 5580. [[CrossRef](#)]
61. Li, M.L.; Yin, L.C.; Zhang, Y.; Su, X.K.; Liu, G.H.; Wang, X.F.; Au, Y.; Wu, X. Spatio-temporal dynamics of fractional vegetation coverage based on MODIS-EVI and its driving factors in Southwest China. *Acta Ecol. Sin.* **2021**, *41*, 1138–1147. (In Chinese)
62. Harris, I.; Osborn, T.; Jones, P.; Lister, D. Version 4 of the CRU TS monthly high-resolution gridded multivariate climate dataset. *Sci. Data* **2020**, *7*, 109. [[CrossRef](#)]
63. Buermann, W.G.; Forkel, M.; O’Sullivan, M.; Sitch, S.; Friedlingstein, P.; Haverd, V. Widespread seasonal compensation effects of spring warming on northern plant productivity. *Nature* **2018**, *562*, 110–115. [[CrossRef](#)]
64. Wen, X.; Wang, S.; Zhu, J.; David, V. An Overview of China Climate Change over the 20th Century Using UK UEA/CRU High Resolution Grid Data. *Chin. J. Atmos. Sci.* **2006**, *30*, 894–904. (In Chinese)
65. Knott, G.D. *Interpolating Cubic Splines*; Springer Science & Business Media: Berlin, Germany, 2012; pp. 1–244.
66. Wang, M.; An, Z. Quantifying the Interaction Effects of Climatic Factors on Vegetation Growth in Southwest China. *Remote Sens.* **2023**, *15*, 774. [[CrossRef](#)]
67. Xiong, Q.L.; He, Y.L.; Deng, F.Y.; Li, T.Y.; Yu, L. Assessment of alpine mean response to climate change in Southwest China based on MaxEnt model. *Acta Ecol. Sin.* **2019**, *39*, 9033–9043. (In Chinese)
68. Wang, X.H.; Piao, S.L.; Ciais, P.; Li, J.S.; Friedlingstein, P.; Koven, C.D.; Chen, A.P. Spring temperature change and its implication in the change of vegetation growth in North America from 1982 to 2006. *Proc. Natl. Acad. Sci. USA* **2011**, *108*, 1240–1245. [[CrossRef](#)]
69. Smith, T.M.; Reynolds, R.W.; Peterson, T.C.; Lawrimore, J. Improvements to NOAA’s historical merged land-ocean surface temperature analysis (1880–2006). *J. Clim.* **2008**, *21*, 2283–2296. [[CrossRef](#)]
70. Zhu, X.; Dong, W.; Wei, Z.; Guo, Y.; Gao, X.; Wen, X.; Yang, S.; Zheng, Z.; Yan, D.; Zhu, Y.; et al. Multi-decadal evolution characteristics of global surface temperature anomaly data shown by observation and CMIP5 models. *Int. J. Climatol.* **2017**, *38*, 1533–1542. [[CrossRef](#)]
71. Kosaka, Y.; Xie, S. Recent global-warming hiatus tied to equatorial Pacific surface cooling. *Nature* **2013**, *501*, 403–407. [[CrossRef](#)] [[PubMed](#)]
72. Cai, Y.; Li, D.L.; Tang, M.C.; Bai, C.Y. Decadal temperature changes over Qinghai-Xizang plateau in recent 50 years. *Plateau Meteorol.* **2003**, *22*, 464–470. (In Chinese with English abstract)
73. Liu, X.; Chen, B. Climatic warming in the Tibetan plateau during recent decades. *Int. J. Climatol.* **2000**, *20*, 1729–1742. [[CrossRef](#)]

74. Wang, H.; Liu, H.; Cao, G.; Sanders, N.J.; Classen, A.T.; He, J.S. Alpine grassland plants grow earlier and faster but biomass remains unchanged over 35 years of climate change. *Ecol. Lett.* **2020**, *23*, 701–710. [[CrossRef](#)]
75. Li, L.; Chen, X.G.; Wang, Z.Y.; Xu, W.X.; Tang, H.Y. Climate change and its regional differences over the tibetan plateau. *Adv. Clim. Chang. Res.* **2010**, *6*, 181–186. (In Chinese with English abstract)
76. Oguntunde, P.G.; Abiodun, B.J.; Lischeid, G. Rainfall trends in Nigeria, 1901–2000. *J. Hydrol.* **2011**, *411*, 207–218. [[CrossRef](#)]
77. Li, Y.P.; Chen, Y.N.; Li, Z. Dry/wet pattern changes in global dryland areas over the past six decades. *Glob. Planet. Chang.* **2019**, *178*, 184–192. [[CrossRef](#)]
78. Sun, W.B.; Li, Q.X.; Huang, B.Y.; Cheng, J.Y.; Song, Z.Y.; Li, H.Y.; Dong, W.J.; Zhai, P.M.; Jones, P.D. The Assessment of Global Surface Temperature Change from 1850s: The C-LSAT2.0 Ensemble and the CMST-Interim Datasets. *Adv. Atmos. Sci.* **2021**, *38*, 875–888. [[CrossRef](#)]
79. Roderick, M.L.; Sun, F.; Lim, W.H.; Farquhar, G.D. A general framework for understanding the response of the water cycle to global warming over land and ocean. *Hydrol. Earth Syst. Sci.* **2014**, *18*, 1575–1589. [[CrossRef](#)]
80. Bonan, G.B. Forests and climate change: Forcings, feedbacks, and the climate benefits of forests. *Science* **2008**, *320*, 1444–1449. [[CrossRef](#)]
81. Yang, K.; Ye, B.S.; Zhou, D.G.; Wu, B.Y.; Foken, T.; Qin, J.; Zhou, Z.Y. Response of hydrological cycle to recent climate changes in the Tibetan Plateau. *Clim. Chang.* **2011**, *109*, 517–534. [[CrossRef](#)]
82. Dong, N.; Xu, X.D.; Cai, W.Y.; Zhao, T.L.; Sun, C. Comprehensive effects of interdecadal change of sea surface temperature increase in the Indo-Pacific Ocean on the warming-wetting of the Qinghai–Tibet Plateau. *Sci. Rep.* **2022**, *12*, 22306. [[CrossRef](#)] [[PubMed](#)]
83. Ren, Q.; Zhou, C.Y.; He, J.H.; Cen, S.X.; Deng, M.Y. Impact of preceding Indian Ocean Sea surface temperature anomaly on water vapor content over the Tibetan Plateau moist pool in summer and its possible reason. *Chin. J. Atmos. Sci.* **2017**, *41*, 648–658.
84. Tang, J.; Guo, X.L.; Chang, Y.; Lu, G.X.; Qi, P. Temporospatial distribution and trends of thunderstorm, hail, gale, and heavy precipitation events over the Tibetan Plateau and associated mechanisms. *J. Clim.* **2021**, *34*, 9623–9646. [[CrossRef](#)]
85. Li, L.; Zhang, R.H.; Wen, M.; Lv, J.M. Regionally different precipitation trends over the Tibetan Plateau in the warming context: A perspective of the Tibetan Plateau vortices. *J. Geophys. Res.* **2021**, *48*, 1680. [[CrossRef](#)]
86. Yao, T.; Thompson, L.; Yang, W.; Xiang, Y.; Kattel, D.B.; Joswiak, D. Different glacier status with atmospheric circulations in Tibetan Plateau and surroundings. *Nat. Clim. Chang.* **2012**, *2*, 663–667. [[CrossRef](#)]
87. Zhao, H.; Xu, B.; Yao, T.; Wu, G.; Lin, S.; Gao, J.; Wang, M. Deuterium excess record in a southern Tibetan ice core and its potential climatic implications. *Clim. Dynam.* **2012**, *38*, 1791–1803. [[CrossRef](#)]
88. Norris, J.; Carvalho, L.M.V.; Jones, C.; Cannon, F. Warming and drying over the central Himalaya caused by an amplification of local mountain circulation. *Npj Clim. Atmos. Sci.* **2020**, *3*, 1. [[CrossRef](#)]
89. Sun, J.; Yang, K.; Guo, W.D.; Wang, Y.; He, J.; Lu, H. Why has the Inner Tibetan Plateau become wetter since the mid-1990s? *J. Clim.* **2020**, *33*, 8507–8522. [[CrossRef](#)]
90. Zhang, C.; Tang, Q.; Chen, D. Recent changes in the moisture source of precipitation over the Tibetan Plateau. *J. Clim.* **2017**, *30*, 1807–1819. [[CrossRef](#)]
91. Curio, J.; Maussion, F.; Scherer, D. A 12-year high-resolution climatology of atmospheric water transport over the Tibetan Plateau. *Earth Syst. Dyn.* **2015**, *6*, 109–124. [[CrossRef](#)]
92. Yao, J.Q.; Yang, Q.; Mao, W.Y.; Zhao, Y.; Xu, X.B. Precipitation trend–Elevation relationship in arid regions of the China. *Glob. Planet. Chang.* **2016**, *143*, 1–9. [[CrossRef](#)]
93. Tu, J.; Lu, E. Relative importance of water vapor and air temperature in the interannual variation of the seasonal precipitation: A comparison of the physical and statistical methods. *Clim. Dyn.* **2020**, *54*, 3655–3670. [[CrossRef](#)]
94. Ding, Y.H.; Sun, Y.; Wang, Z.Y.; Song, Y.F. Inter-decadal variation of the summer precipitation in China and its association with decreasing Asian summer monsoon Part II: Possible causes. *Int. J. Climatol.* **2009**, *29*, 1926–1944. [[CrossRef](#)]
95. Hu, Y.; Xu, J.; Huang, C.; Zhou, Y.; Pang, Y.; Shi, Z.; Chen, X. Spatial and Temporal Variations in the Rainy Season Onset over the Qinghai–Tibet Plateau. *Water* **2019**, *11*, 1960. [[CrossRef](#)]
96. Liu, Z.; Yang, M.; Wan, G.; Wang, X. The Spatial and Temporal Variation of Temperature in the Qinghai-Xizang (Tibetan) Plateau during 1971–2015. *Atmosphere* **2017**, *8*, 214. [[CrossRef](#)]
97. Wang, S.J. Spatiotemporal variability of temperature trends on the southeast Tibetan Plateau, China. *Int. J. Climatol.* **2018**, *38*, 11953–11963. [[CrossRef](#)]
98. Chen, L.X.; Song, Y.K.; Liu, J.P.; Wang, W. On the diurnal variation of convection over Qinghai-Xizang Plateau during summer as revealed from meteorological satellite data. *Acta Meteorol. Sin.* **1999**, *57*, 549–560.
99. Xu, X.K. Spatiotemporal variation of total cloud and low cloud over China. *Meteorol. Mon.* **2012**, *38*, 90–95.
100. Shen, M.G.; Piao, S.L.; Jeong, S.J.; Zhang, G.X.; Zhang, Y.J.; Yao, T.D. Evaporative cooling over the Tibetan Plateau induced by vegetation growth. *Proc. Natl. Acad. Sci. USA* **2015**, *112*, 9299–9304. [[CrossRef](#)] [[PubMed](#)]
101. Pei, J.; Niu, Z.; Wang, L.; Huang, N.; Cao, J.H. Quantifying the Spatio-Temporal Variations and Impact Factors for Vegetation Coverage in the Karst Regions of Southwest China Using Landsat Data and Google Earth Engine. In Proceedings of the Conference on Multispectral, Hyperspectral, and Ultraspectral Remote Sensing Technology, Techniques, and Applications, Honolulu, HI, USA, 23 October 2018.

102. Jackson, R.B.; Randerson, J.T.; Anderson, R.G.; Avissar, R.; Baldocchi, D.D.; Bonan, G.B.; Caldeira, K.; Diffenbaugh, N.S.; Field, C.B.; Hungate, B.A.; et al. Protecting climate with forests. *Environ. Res. Lett.* **2008**, *3*, 044006. [[CrossRef](#)]
103. Chen, S.; Zhang, R.; Mao, R.; Zhang, Y.; Chen, Y.; Ji, Z.; Gong, Y.; Guan, Y. Sources, characteristics and climate impact of light-absorbing aerosols over the Tibetan Plateau. *Earth-Sci. Rev.* **2022**, *232*, 104111. [[CrossRef](#)]
104. Zhang, R.; Zhou, S. The air temperature change over the Tibetan Plateau during 1979–2002 and its possible linkage with ozone depletion. *Acta Meteor. Sin.* **2008**, *6*, 916–925.
105. Yang, X.; Hou, Y.; Chen, B. Observed surface warming induced by urbanization in east China. *J. Geophys. Res.* **2011**, *116*, D14113. [[CrossRef](#)]
106. Duan, A.; Xiao, Z.; Wu, G. Characteristics of climate change over the Tibet Plateau under the global warming during 1979–2014. *Clim. Chang. Res.* **2016**, *12*, 374–381.
107. Wang, M.; Wang, H.S.; Jiang, C.; Sun, J.X. Spatial soil erosion patterns and quantitative attribution analysis in Southwestern China based on RUSLE and Geo-Detector model. *J. Basic Sci. Eng.* **2021**, *29*, 1386–1402. (In Chinese with English abstract)
108. Bao, X.; Zhang, F. How accurate are modern atmospheric reanalysis for the data-sparse Tibetan Plateau region. *J. Clim.* **2019**, *32*, 7153–7172. [[CrossRef](#)]

Disclaimer/Publisher’s Note: The statements, opinions and data contained in all publications are solely those of the individual author(s) and contributor(s) and not of MDPI and/or the editor(s). MDPI and/or the editor(s) disclaim responsibility for any injury to people or property resulting from any ideas, methods, instructions or products referred to in the content.